RESEARCH ARTICLE

WILEY-VCH

Vibrational properties of $LaNb_{0.8}M_{0.2}O_{4-\delta}$ (where M=As, Sb, V, and Ta)

Aleksandra Mielewczyk-Gryń*[a], Sebastian Wachowski[a], Kacper Dzierzgowski[a], Iga Szpunar[a], Judyta Strychalska-Nowak[a], Tomasz Klimczuk[a], Mirosław Sawczak[b], Maria Gazda[a]

[a] Institute of Nanotechnology and Materials Engineering,
Faculty of Applied Physics and Mathematics, and Advanced Materials Centre,
Gdańsk University of Technology
Narutowicza 11/12,
80-233 Gdańsk Poland
E-mail: alegryn@pg.edu.pl

[b] Institute of Fluid Flow Machinery,
Polish Academy of Sciences,
Fiszera 14,
80-231 Gdańsk, Poland

Abstract: $LaNb_{0.8}M_{0.2}O_{4-\delta}$ (where M=As, Sb, V, and Ta) oxides with pentavalent elements of different ionic sizes were synthesized by a solid-state reaction method. The vibrational properties of these oxides have been investigated. These studies revealed that the substituent element influences both Debye temperature value as well as the Raman active vibrational modes. Additionally, the low-temperature vibrational properties of $LaNb_{0.8}Sb_{0.2}O_{4-\delta}$ have been determined to show the phase transition occurrence at 260 K which is lower than previously reported.

Introduction

Rare-earth orthoniobates are a group of ceramics with a variety of properties including ferroelectricity [1–3], optical activity [4], and ionic transport [5,6]. Among this group lanthanum orthoniobates, $LaNbO_4$, are of large interest owing to their potential applications in energy conversion and gas sensing [7,8]. This system can be widely substituted in both lanthanum and niobium sublattices and by this, its properties can be tuned for the desired application. The substitution in the lanthanum sublattice usually is undertaken to either enhance the ionic conductivity (substitutions with Ca [5], Mg [9], or Sr [10]) or photoluminescent properties (substitutions with Eu, Tb) [11,12]. The phase transition from the high temperature tetragonal scheelite structure (space group $I4_1/a$) to the low temperature monoclinic fergusonite (space group I2/c) in lanthanum orthoniobates has been studied by various groups. These studies reports that in the case of undoped material the phase transition occurs at 500°C[3]. The niobium-site substitution is introduced to influence the structure of orthoniobates and either lower (substitutions with V [6], As [13], and Sb [14]) or increase (Ta [15]) the structural phase transition temperature. It has been also reported that for all substitutions, even though the phase transition temperature shifts, the thermodynamic nature of the transition does not change and it retains to be the second order phase transition[3,9,16]. Our previous studies revealed that the substitution in the niobium sublattice with antimony changes the thermal properties. In that case, the decrease of the Debye temperature with increasing antimony content was correlated with decreasing scheelite–fergusonite transition temperature [17]. The current study presents the findings concerning the influence of substitution of lanthanum orthoniobate by four elements, namely arsenic, antimony, vanadium, and tantalum on the vibrational properties of this system. This work adds additional information to the studies of doped lanthanum orthoniobate, it revisits the phase transition temperature study on room temperature stabilized scheelite phase $LaNbO_4$. This is also the first Raman spectroscopy study on Nb-site doped lanthanum orthoniobates and the first to compare material substituted by four different cations (Sb, Ta, V and As).

Results and Discussion

As shown by our previous studies, the $LaNb_{0.8}Sb_{0.2}O_{4-\delta}$, $LaNb_{0.8}Ta_{0.2}O_{4-\delta}$, and $LaNb_{0.8}V_{0.2}O_{4-\delta}$ [5], as well as $LaNb_{0.8}As_{0.2}O_{4-\delta}$ [11] samples, were single-phase orthoniobates, however, the coexistence of the monoclinic and tetragonal crystal structures was observed. In this study, we have carried out a further structural analysis to determine the percentage phase contents of monoclinic fergusonite and tetragonal scheelite phases. Rietveld profiles, as well as experimental diffraction data of the synthesized materials, are presented in Fig. 1. The observed misfit of the reflections around 32° originates from the preferred orientation phenomena, which lead to the increased intensity of the reflections indexed with the 040 (monoclinic structure) and 004 (tetragonal structure) Miller indices[9]. The unit cell parameters and the phase contents are summarized in Tab. 1. One can see that for the samples with different substituents, the phase content varies. The highest content of the tetragonal phase is present in the sample substituted with antimony, while in the sample substituted with tantalum, only the monoclinic phase is present. This reflects the influence of the dopant on the stabilization of either the tetragonal or the monoclinic phase. The transition temperature from the monoclinic to the tetragonal phase is shifted towards lower temperatures for Sb, V, and As, while it is higher for Ta [14,15]. Heat capacity comprises contributions from electronic, harmonic, dilatational, and anharmonic terms. In the present analysis, corrections for dilatation and anharmonicity were not included. The fitting of the low-temperature heat capacity is shown in Fig. 2, where heat capacity divided by temperature is plotted as a function of T^2. Below 8 K the relation: $C_p = \gamma T + \beta T^3$ can be fitted for all samples and the lines intercept the axes at 0 K which suggests the low value of the Sommerfeld (γ) constant. This comes in line with the fact that these compounds are electronic insulators [15,18,19] and the electronic contribution to heat capacity is negligible. Figure 3 presents the calculated Debye temperature dependence on the substituent mass and ionic radii. One can see that the Debye temperature is the highest for arsenic and the lowest for tantalum substitution. This can be linked to the changes in the B-cation-oxygen bond induced by bigger/smaller cation substitution in the niobium lattice which leads to changes in vibrational proprieties of the material.

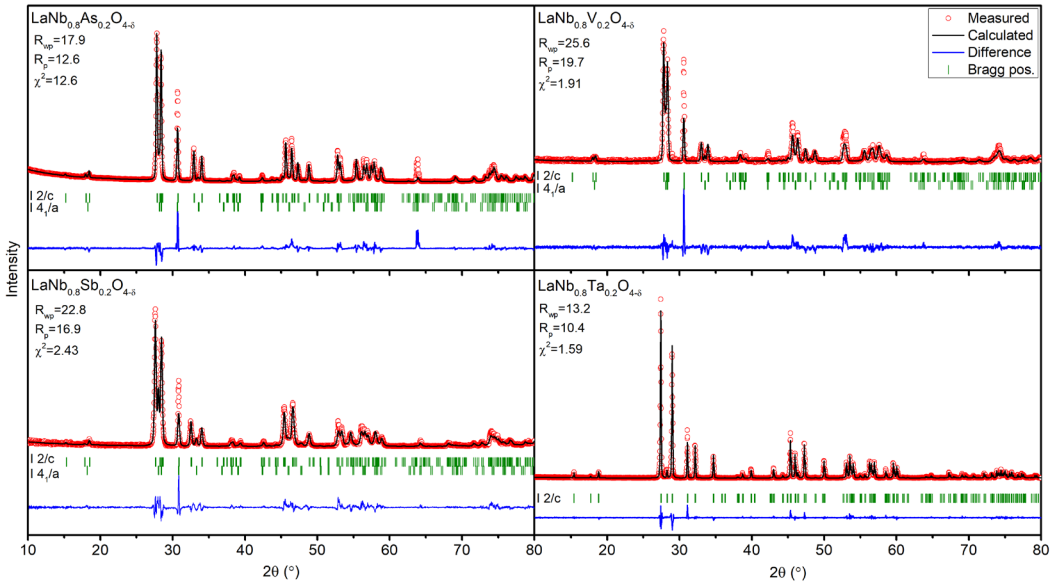

Figure 1. X-ray diffractograms with Rietveld profiles and difference plots for $LaNb_{0.8}M_{0.2}O_{4-\delta}$ (where M=As, Sb, V, and Ta).

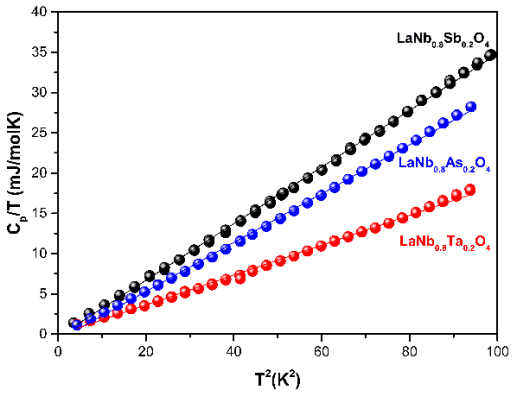

Figure 2. The heat capacity divided by temperature plotted as a function of T^2. The data for $LaNb_{0.8}Sb_{0.2}O_{4-\delta}$ are taken from [17].

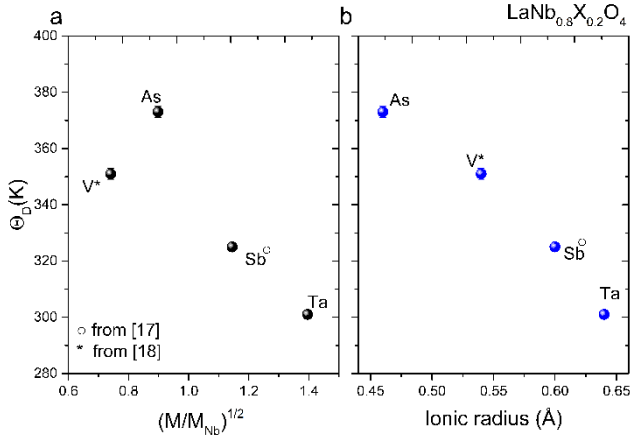

Figure 3. Debye temperature vs the ratio between the substituent element molar mass and the niobium mass (a) and vs ionic radii of substituent element (b). Value for $LaNb_{0.8}V_{0.2}O_{4-\delta}$ and for $LaNb_{0.8}Sb_{0.2}O_{4-\delta}$ after [20] and [17].

It has been previously reported for both vanadium and antimony [17,20] that the higher Debye temperature is observed in the orthoniobates with the higher temperature of the structural phase transition. However, in this case, tantalum substitution leads to the lowest Debye temperature, whereas the structural transition temperature is the highest. This suggests that the Debye temperature is affected by the introduction of the substituent with a particular ionic radius and molar mass but does not collate with the phase transition temperature. This would suggest that although the substitution changes the structural features and stabilizes a particular structure, the vibrational properties are rather linked to the effective ionic radii and mass of the cations in the niobium sublattice. Therefore, it seems that the smaller substituent is the stiffer the lattice becomes. The stiffening may be the result of strain introduced by cation size variance or the different strength of the bonds formed by the substituents. To check whether it is the bond strength of the B-O bonds which affects the Debye temperature, one may compare Bond Dissociation Energies (BDEs) of the bonds between substituents and oxygen to evaluate their potential bond strength. BDEs for Ta-O, Sb-O, V-O, and As-O are respectively 839, 434, 637, and 484 kJ/mol [21]. This vast variation of bond energy shows that the overall stiffness of the whole crystal lattice does not depend on these particular bonds. So, we suggest that it is the size mismatch and related strain of the crystal lattice which are the factors controlling the Debye temperature. This hypothesis is also supported by our previous studies in which we reported that both Debye temperature and spontaneous strain in the crystal lattice are decreasing as a function of Sb content [16,17]. Moreover, Zhang et al. studied Debye temperature variation in $Gd_2Zr_2O_7$-$Sm_2Zr_2O_7$ solid solution and their calculations show that the introduction of samarium with a bigger ionic radius into the zirconium sublattice is reflected in the lowering of the Debye temperature [22]. The results of the molar mass dependence are also in line with our previous findings for antimony substitution in lanthanum orthoniobate which have shown that the Debye temperature gradually lowers for higher antimony content which is also linked to higher average molar mass in niobium sublattice [17]. Therefore, the Debye temperature to some degree depends on the mass of the substituent as the higher mass softens the vibrations but this effect is weaker than the size mismatch and therefore the bong lengths in respective tetrahedra. This is in the agreement with Nakamura, studies who reported dependencies of both molar mass and equilibrium interionic distance with Debye temperature for multiple ionic and covalent compounds [23].

Raman spectroscopy was performed to investigate the vibrational modes of the substituted LNO samples. The results obtained are depicted in Fig. 4. As was previously reported for both $RENbO_4$ and $REVO_4$, the vibrational modes of these structures can be divided into the one being associated with the vibration of RE cation and niobium/vanadium tetrahedra [24–27]. The primitive unit cell in the fergusonite structure (space group I2/a, C2h) contains two formula units, giving rise to 36 vibrational modes. Normal modes at the center of the Brillouin zone might be classified according to the subsequent irreducible representations: $\Gamma=8A_g+8A_u+10B_g+10B_u$ One A_u and two B_g modes are acoustic modes [28].

Table 1. Phase composition and lattice parameters of $LaNb_{0.8}M_{0.2}O_4$, where M = V, Sb, As, Ta. Parameters with index $_m$ characterizes the monoclinic phase lattice parameters, while the index $_t$ characterizes the tertragonal structure lattice parameters.

Composition	Monoclinic phase (I2/c) content (%)	Tetragonal phase (I41/a) content (%)	a_m (Å)	b_m (Å)	c_m (Å)	β_m (°)	a_t (Å)	c_t (Å)
$LaNb_{0.8}V_{0.2}O_4$	91(1)	9(1)	5.4254(2)	11.6818(5)	5.2826(1)	91.463(2)	5.3493(4)	11.6846(18)
$LaNb_{0.8}Sb_{0.2}O_4$	86(1)	14(1)	5.5065(2)	11.5935(5)	5.271(2)	92.436(2)	5.3839(6)	11.6064(1)
$LaNb_{0.8}As_{0.2}O_4$	93(1)	7(1)	5.4374(1)	11.6464(2)	5.2683(1)	91.705(1)	5.3397(8)	11.667(32)
$LaNb_{0.8}Ta_{0.2}O_4$	100	-	5.5817(1)	11.5018(1)	5.1867(1)	94.516(1)	-	-

The structure is centrosymmetric. All even (*g*) modes are Raman active, while every optic odd (*u*) mode is infrared active. *A* (*B*) modes are symmetric (antisymmetric) concerning the two-order axis [29]. The observed vibrational modes present good agreement with other studies reported in the literature [24,27,30]. Lanthanum orthoniobate has monoclinic symmetry and when unsubstituted can be considered as being formed by tetrahedral NbO_4^{3-} groups and La^{3+} ions, where the modes below 300 cm^{-1} can be associated with La^{3+} ions present in the crystal lattice, as well as, movement of the niobate molecule as a rigid unit [31]. The additional higher modes can be related as follows: the mode around 330 cm^{-1} (v_2) can be recognized as the symmetric deformation of the tetrahedron NbO_4^{3-} (scissors mode of NbO_4^-) [2]; those at 395 and 420 cm^{-1} (v_4) can be assigned to asymmetric deformations in the tetrahedral structure; those at 625 and 665 cm^{-1} (v_3) can be assigned to the antisymmetric Nb–O stretching, and the mode at 802cm^{-1} (v_1) can be associated to the symmetric stretching of Nb–O bonds in the tetrahedron. [27]. For tetragonal scheelite, structure representation is given as $\Gamma=3A_g+5A_u+5B_g+3B_u+5E_g+5E_u$ where all A_g, B_g, and E_g are Raman active. All vibrational modes can be associated with particular A and B molecular symmetry species as indicated in Figure 4.

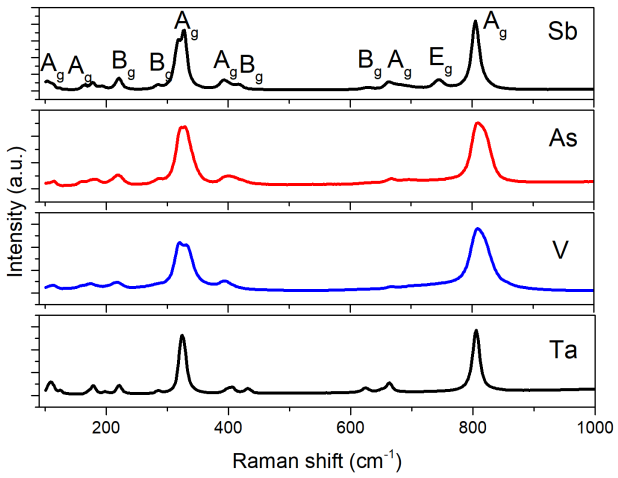

Figure 4. Raman spectra collected at room temperature for all studied compositions.

In the case of our study, the major differences in the spectra for particular compositions originate from niobium site substitution. Therefore, we expect to see differences mainly for vibrational modes at approximately 325 cm^{-1} originating from the symmetric deformation of the tetrahedra and around 805 cm^{-1} being associated with the symmetric stretching of the Nb-O bonds. In these regions, two separate bands with A_g symmetry can be recognized (Figure 5) [2]. The changes in relative intensity of the bands associated with these modes can be attributed to the sample structure and the existing preferred orientation resulting from the substitution (Table 2). The splitting is present in the samples with the tetragonal phase content. Moreover, the splitting is more pronounced in the compounds with a higher content of the tetragonal phase. This reflects the presence of both niobium-oxygen tetrahedra of the monoclinic phase and niobium-oxygen octahedra of the tetragonal phase. In the tetragonal structure, oxygen ions form a regular tetrahedron around Nb^{5+}, in the monoclinic structure NbO_x polyhedra are often considered to be intermediate between isolated tetrahedra and edge-sharing chains of NbO_6 octahedra with two long Nb-O bonds [32]. It is also worth noting that the only sample without the clear band splitting is the one with tantalum, which is the only single-phase monoclinic sample. This spectrum is also the most similar to the one of the unsubstituted $LaNbO_4$ reported by Nascimento et al. [27]. Similar spectra characteristics below 300 cm^{-1} for all studied samples to one of the undoped materials are related to the association of these modes with La^{3+} ions present in the crystal lattice so this should not vary much because of the niobium site substitution. Moreover, the sample with the highest amount of tetragonal phase ($LaNb_{0.8}Sb_{0.2}O_4$) has a visible E_g mode which is absent for other compositions.

The FWHM for most intense modes, above 300 cm^{-1}, changes with the substitution. This reflects the changes in the rigidity of the NbO_4 tetrahedron. Saying that in for the mode resulting from stretching of the Nb(M)-O bond (330 cm^{-1}) the FWHM is the widest for vanadium samples and the thinnest for antimony and tantalum samples (Tab. 2). The changes in the rigidity of Nb(M)-O should be also attributed to structural changes induced by substitution. Previous studies on vanadium substituted $LaNbO_4$ showed that the force constant between the nearest (Nb, V)O_4 tetrahedral units softens at T_c as a function of vanadium content, this supports the link between phase content and vibrational modes visible for other substituents [33]. To investigate how the phase transition is reflected in Raman spectra the low-temperature studies of $LaNb_{0.7}Sb_{0.3}O_4$ have been undertaken. The result of this study is presented in Figure 6(a). According to our previous studies, the structural transition temperature of $LaNb_{0.7}Sb_{0.3}O_4$ is in the range of 280 to 300 K [34].As it is shown in Fig. 7(b), with the lowering temperature, some changes in the region of 330 cm^{-1} can be seen. Below approximately 260 K the relative intensity of two components of the split peak around 330 cm^{-1} changes which reflects the changes in the structure of the sample. Similar results have been reported for $LaTaO_4$ before [35]. Moreover, Ishii et al. observed a small discontinuity at 279 K in the time evolution of the width of a small-wave number Raman band under stress, and

credited this to the cooperative relaxation in the freshly extended region of a ferroelastic domain [2] and can be associated with ferroelastic phase transition. Since the change is below 260 K one can assume that the temperature of phase transition can be lower than reported previously. This discrepancy can arise from the fact that in the case of diffraction studies the results reflect the average structure of the oxide. In the case of Raman studies, the studied sample is much smaller and therefore the temperature equilibrium is easier to achieve.

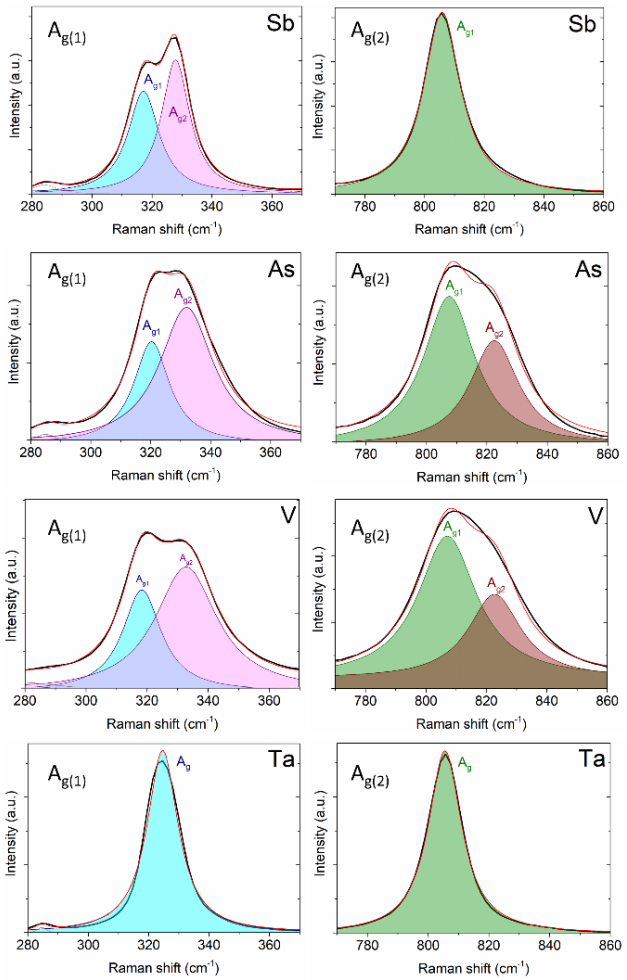

Figure 5. Raman spectra's deconvolution containing of raw data (red line), envelope (black line) and spectral components (color fields).

Moreover, Raman spectroscopy is far more structure sensitive, in the case of this system, than X-ray diffraction and the Raman modes can be affected by smaller tetragonal phase quantities [36]. Furthermore, this method is far more sensitive for short-range and local ordering, hence, the difference in the results obtained with x-ray diffraction in our previous work.

Conclusion

The lanthanum orthoniobate samples with different substitutions leading to stabilization of either low (tantalum) or high temperature (antimony, vanadium, arsenic) polymorph have been synthesized and their low-temperature thermodynamic properties have been measured. The dependence on substitution of Debye temperature has been established as well as the influence on structural features reflected in the vibrational properties. The relation between ionic radii and Debye temperature reflects the changes in the vibrational properties induced by doping. A similar relation is visible in changes in Raman modes between samples substituted by different elements. Moreover, the phase transition temperature of $LaNb_{0.7}Sb_{0.3}O_4$ has been established based on Raman spectroscopy measurement to be as low as 260 K which is lower than previously reported [34].

Experimental Section

The samples of $LaNb_{0.8}M_{0.2}O_{4-\delta}$ (where M=As, Sb, V, and Ta) have been synthesized by a standard two-step solid-state synthesis described elsewhere[19,37]. The phase composition of the synthesized samples was checked with powder X-ray diffraction (PXRD) using Cu-Kα radiation. Room temperature measurements were performed on a Phillips X'Pert Pro MPD diffractometer in the 2θ range of 10–120°. The XRD patterns were analyzed by the Rietveld refinement procedure, as implemented in the FullProf software suite [38]. Starting models were based on the monoclinic fergusonite (I2/c) [39] and tetragonal scheelite (I41/a) [40] structures of LaNbO4. Heat capacity measurements (thermal relaxation technique) in the temperature range 2<T<300 K were carried out using a Quantum Design Physical Property Measurement System (PPMS). Raman spectra were recorded using the micro-Raman spectrometer (InVia, Renishaw) equipped with liquid nitrogen cryostats (MicrostatN, Oxford Instruments) controlled with a temperature controller (Mercury ITC, Oxford Instruments). Raman spectra were recorded under excitation at 514 nm, with an Argon-ion laser. Samples were analyzed in a temperature range from 320 to 100 K with 20 K temperature intervals. Each Raman spectrum was averaged over 3 accumulations to improve the signal-to-noise ratio.

Acknowledgements

The study was supported by a grant from the Ministry of Science and Higher Education, Poland Grant No IP2015 051374.

Keywords: lanthanum orthoniobate • phase transitions • Raman spectroscopy • heat capacity

Table 2. Peak parameters of the deconvoluted spectra

	$A_{g(1)}$					$A_{g(2)}$				
	$A_{g(1)1}$		$A_{g(1)2}$			$A_{g(2)1}$		$A_{g(2)2}$		
	Position (cm^{-1})	FWHM (cm^{-1})	Position (cm^{-1})	FWHM (cm^{-1})	Relative intensity $A_{g(1)1}/ A_{g(1)2}$	Position (cm^{-1})	FWHM (cm^{-1})	Position (cm^{-1})	FWHM (cm^{-1})	Relative intensity $A_{g(2)1}/ A_{g(2)2}$
Sb	317	13	328	13	0.77	806	15	-	-	-
As	320	15	332	22	0.74	808	21	823	20	1.44
V	318	15	333	25	0.81	807	24	823	21	1.62
Ta	325	13	-	-	-	806	13	-	-	-

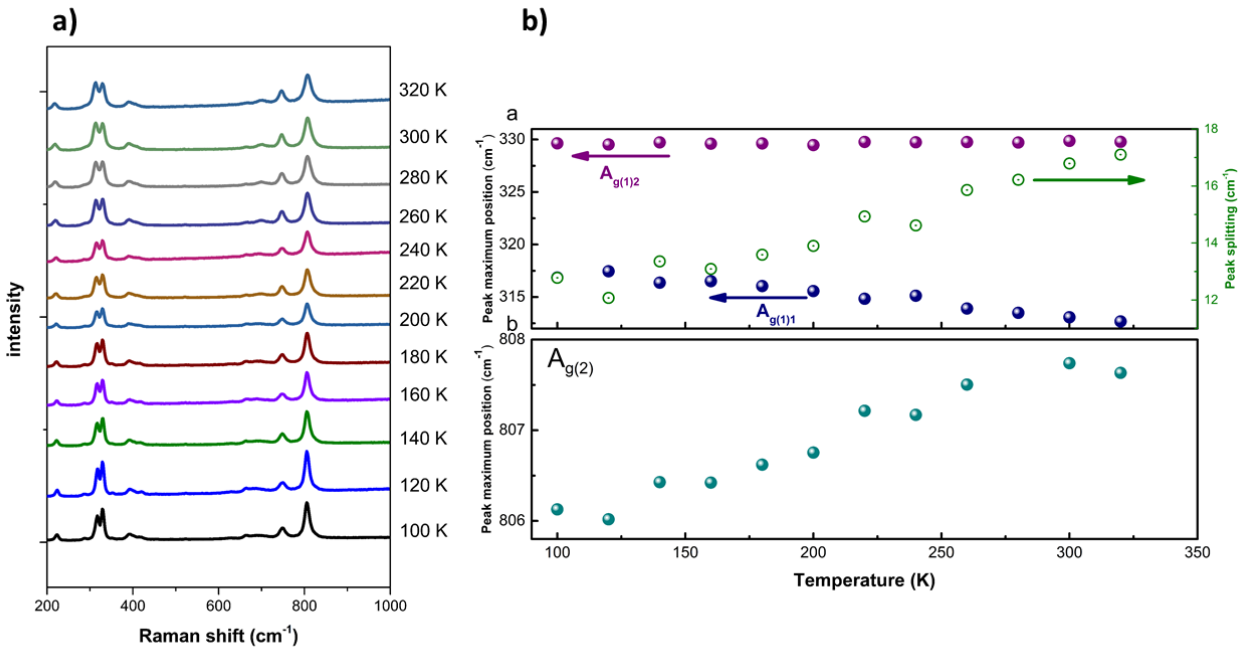

Figure 6 (a) Raman spectra collected at temperature range 100-320 K for antimony substituted lanthanum orthoniobate ($LaNb_{0.7}Sb_{0.3}O_4$). (b) Temperature dependencies of peak maximum positions and peak splitting for antimony substituted lanthanum orthoniobate ($LaNb_{0.7}Sb_{0.3}O_4$).

[1] L. H. Brixner, J. F. Whitney, F. C. Zumsteg, G. A. Jones, *Mater. Res. Bull.* **1977**, *12*, 17–24.
[2] K. Ishii, N. Morita, H. Nakayama, S. Tsunekawa, T. Fukuda, *Phys. Status Solidi* **1989**, *112*, 207–214.
[3] K. Hara, A. Sakai, S. Tsunekawa, A. Sawada, Y. Ishibashi, T. Yagi, *J. Phys. Soc. Japan* **1985**, *54*, 1168–1172.
[4] G. Blasse, A. Bril, *J. Lumin.* **1970**, *3*, 109–131.
[5] R. Haugsrud, T. Norby, *Nat Mater* **2006**, *5*, 193–196.
[6] M. E. Ivanova, W. a. Meulenberg, J. Palisaitis, D. Sebold, C. Solís, M. Ziegner, J. M. Serra, J. Mayer, M. Hänsel, O. Guillon, *J. Eur. Ceram. Soc.* **2014**, *35*, 1–15.
[7] H. Fjeld, K. Toyoura, R. Haugsrud, T. Norby, *Phys. Chem. Chem. Phys.* **2010**, *12*, 10313–9.
[8] A. Magrasó, M.-L. Fontaine, Y. Larring, R. Bredesen, G. E. Syvertsen, H. L. Lein, T. Grande, M. Huse, R. Strandbakke, R. Haugsrud, T. Norby, *Fuel Cells* **2011**, *11*, 17–25.
[9] A. Mielewczyk-Gryn, K. Gdula-Kasica, B. Kusz, M. Gazda, *Ceram. Int.* **2013**, *39*, 4239–4244.
[10] C. Li, S. S. Pramana, N. Ni, J. Kilner, S. J. Skinner, *ACS Appl. Mater. Interfaces* **2017**, *9*, 29633–29642.
[11] J. Huang, L. Zhou, Z. Liang, F. Gong, J. Han, R. Wang, *J. Rare Earths* **2010**, *28*, 356–360.
[12] B. Yan, X. Z. Xiao, *Opt. Mater. (Amst).* **2006**, *28*, 498–501.
[13] S. L. Wachowski, B. Kamecki, P. Winiarz, K. Dzierzgowski, M. Jurkowski, J. Dzisevič, A. Mielewczyk-Gryń, M. Gazda, *ChemistrySelect* **2019**, *4*, 8645–8651.
[14] S. Wachowski, A. Mielewczyk-Gryn, M. Gazda, *J. Solid State Chem.* **2014**, *219*, 201–209.
[15] F. Vullum, F. Nitsche, S. M. Selbach, T. Grande, *J. Solid State Chem.* **2008**, *181*, 2580–2585.
[16] A. Mielewczyk-Gryn, S. Wachowski, K. I. Lilova, X. Guo, M. Gazda, A. Navrotsky, *Ceram. Int.* **2015**, *41*, 2128–2133.
[17] A. Mielewczyk-Gryn, S. Wachowski, J. Strychalska, K. Zagórski, T. Klimczuk, A. Navrotsky, M. Gazda, *Ceram. Int.* **2016**, *42*, 7054–7059.
[18] S. S. Bhella, V. Thangadurai, *J. Power Sources* **2009**, *186*, 311–319.
[19] S. Wachowski, A. Mielewczyk-Gryn, K. Zagorski, C. Li, P. Jasinski, S. J. Skinner, R. Haugsrud, M. Gazda, *J. Mater. Chem. A* **2016**, *4*, 11696–11707.
[20] M. Nevitt, G. Knapp, *J. Phys. Chem. Solids* **1986**, *47*, 501–505.
[21] Y.-R. Luo, *Comprehensive Handbook of Chemical Bond Energies*, CRC Press, **2007**.
[22] S. Zhang, H. B. Zhang, F. A. Zhao, M. Jiang, H. Y. Xiao, Z. J. Liu, X. T. Zu, *Sci. Rep.* **2017**, *7*
[23] T. Nakamura, *Jpn. J. Appl. Phys.* **1981**, *20*, L653–L656.
[24] G. S. Freiria, A. L. Ribeiro, M. Verelst, E. J. Nassar, L. A. Rocha, *J. Braz. Chem. Soc.* **2018**, *29*, 594–601.
[25] C. C. Santos, E. N. Silva, A. P. Ayala, I. Guedes, P. S. Pizani, C.-K. Loong, L. A. Boatner, *J. Appl. Phys.* **2007**, *101*, 053511.
[26] I. Guedes, Y. Hirano, M. Grimsditch, N. Wakabayashi, C.-K. Loong, L. A. Boatner, *J. Appl. Phys.* **2001**, *90*, 1843–1846.
[27] J. P. C. do Nascimento, A. J. M. Sales, D. G. Sousa, M. A. S. da Silva, S. G. C. Moreira, K. Pavani, M. J. Soares, M. P. F. Graça, J. Suresh Kumar, A. S. B. Sombra, *RSC Adv.* **2016**, *6*, 68160–68169.
[28] D. Zhou, H.-H. Guo, M. Sen Fu, X. Yao, H. Lin, W. Liu, L.-X. Pang, charanjeet singh, S. Trukhanov, A. Trukhanov, I. M. Reaney, *Inorg. Chem. Front.* **2020**,
[29] J. Pellicer-Porres, A. B. Garg, D. Vázquez-Socorro, D. Martínez-García, C. Popescu, D. Errandonea, *J. Solid State Chem.* **2017**, *251*, 14–18.
[30] J. Hou, Q. Chen, C. GaO, R. Dai, J. Zhang, Z. Wang, Z. Zhang, Z. Ding, *J. Rare Earths* **2014**, *32*, 787–791.
[31] B. G. Mullens, M. Avdeev, H. E. A. Brand, S. Mondal, G. Vaitheeswaran, B. J. Kennedy, *Dalt. Trans.* **2021**, *50*, 9103–9117.
[32] S. Tsunekawa, T. Kamiyama, K. Sasaki, H. Asano, T. Fukuda, *Acta Crystallogr. Sect. A Found. Crystallogr.* **1993**, *49*, 595–600.
[33] A. T. Aldred, S. K. Chan, M. H. Grimsditch, M. V. Nevitt, in *Mater. Res. Soc. Symp. Proc.*, Cambridge University Press, **1984**, pp. 81–86.
[34] A. Mielewczyk-Gryń, S. Wachowski, A. Witkowska, K. Dzierzgowski, W. Skubida, K. Świerczek, A. Regoutz, D. J. Payne, S. Hull, H. Zhang, I. Abrahams, M. Gazda, *J. Am. Ceram. Soc.* **2020**, jace.17352.
[35] Y. G. Abreu, K. P. F. Siqueira, F. M. Matinaga, R. L. Moreira, A. Dias, *Ceram. Int.* **2017**, *43*, 1543–1551.
[36] P. Stacey, S. Hall, S. Stagg, F. Clegg, C. Sammon, *J. Raman Spectrosc.* **2021**, *52*, 1095–1107.
[37] S. Wachowski, B. Kamecki, P. Winiarz, K. Dzierzgowski, A. Mielewczyk-Gryń, M. Gazda, *Inorg. Chem. Front.* **2018**, *5*, 2157–2166.

[38] J. Rodríguez-carvajal, *Recent Developments for the Program FULLPROF*, **2001**.
[39] S. Tsunekawa, H. Takei, M. Ishigame, *Mater. Res. Bull.* **1977**, *12*, 1087–1094.
[40] W. I. F. David, *Mater. Res. Bull.* **1983**, *18*, 749–756.

Entry for the Table of Contents

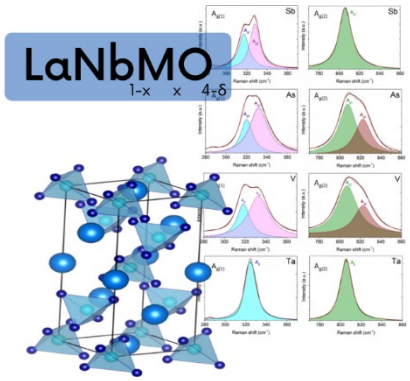

The paper focuses on vibrational properties of isovalent substituted lanthanum orthoniobate studied by the means of low temperature heat capacity measurements and Raman spectroscopy.

Institute and/or researcher Twitter usernames: @leksie_gryn